STARS

University of Central Florida
STARS

Faculty Bibliography 2010s | Faculty Bibliography

1-1-2014

Surface and grain boundary scattering in nanometric Cu thin films: A quantitative analysis including twin boundaries

Katayun Barmak

Amith Darbal

Kameswaran J. Ganesh

Paulo J. Ferreira

Jeffrey M. Rickman

See next page for additional authors

Find similar works at: https://stars.library.ucf.edu/facultybib2010
University of Central Florida Libraries http://library.ucf.edu

This Article is brought to you for free and open access by the Faculty Bibliography at STARS. It has been accepted for inclusion in Faculty Bibliography 2010s by an authorized administrator of STARS. For more information, please contact STARS@ucf.edu.

Recommended Citation

Barmak, Katayun; Darbal, Amith; Ganesh, Kameswaran J.; Ferreira, Paulo J.; Rickman, Jeffrey M.; Sun, Tik; Yao, Bo; Warren, Andrew P.; and Coffey, Kevin R., "Surface and grain boundary scattering in nanometric Cu thin films: A quantitative analysis including twin boundaries" (2014). *Faculty Bibliography 2010s*. 5030.
https://stars.library.ucf.edu/facultybib2010/5030

Authors
Katayun Barmak, Amith Darbal, Kameswaran J. Ganesh, Paulo J. Ferreira, Jeffrey M. Rickman, Tik Sun, Bo Yao, Andrew P. Warren, and Kevin R. Coffey

This article is available at STARS: https://stars.library.ucf.edu/facultybib2010/5030

Surface and grain boundary scattering in nanometric Cu thin films: A quantitative analysis including twin boundaries

Katayun Barmak, Amith Darbal, Kameswaran J. Ganesh, Paulo J. Ferreira, Jeffrey M. Rickman, Tik Sun, Bo Yao, Andrew P. Warren, and Kevin R. Coffey

Citation: Journal of Vacuum Science & Technology A **32**, 061503 (2014); doi: 10.1116/1.4894453
View online: https://doi.org/10.1116/1.4894453
View Table of Contents: https://avs.scitation.org/toc/jva/32/6
Published by the American Vacuum Society

ARTICLES YOU MAY BE INTERESTED IN

Electron mean free path in elemental metals
Journal of Applied Physics **119**, 085101 (2016); https://doi.org/10.1063/1.4942216

Influence of phonon, geometry, impurity, and grain size on Copper line resistivity
Applied Physics Letters **89**, 113124 (2006); https://doi.org/10.1063/1.2355435

Resistivity dominated by surface scattering in sub-50 nm Cu wires
Applied Physics Letters **96**, 042116 (2010); https://doi.org/10.1063/1.3292022

Alteration of Cu conductivity in the size effect regime
Journal of Vacuum Science & Technology B: Microelectronics and Nanometer Structures Processing, Measurement, and Phenomena **22**, 240 (2004); https://doi.org/10.1116/1.1642639

Influence of surface and grain-boundary scattering on the resistivity of copper in reduced dimensions
Applied Physics Letters **84**, 2838 (2004); https://doi.org/10.1063/1.1703844

Size effects and charge transport in metals: Quantum theory of the resistivity of nanometric metallic structures arising from electron scattering by grain boundaries and by rough surfaces
Applied Physics Reviews **4**, 011102 (2017); https://doi.org/10.1063/1.4974032

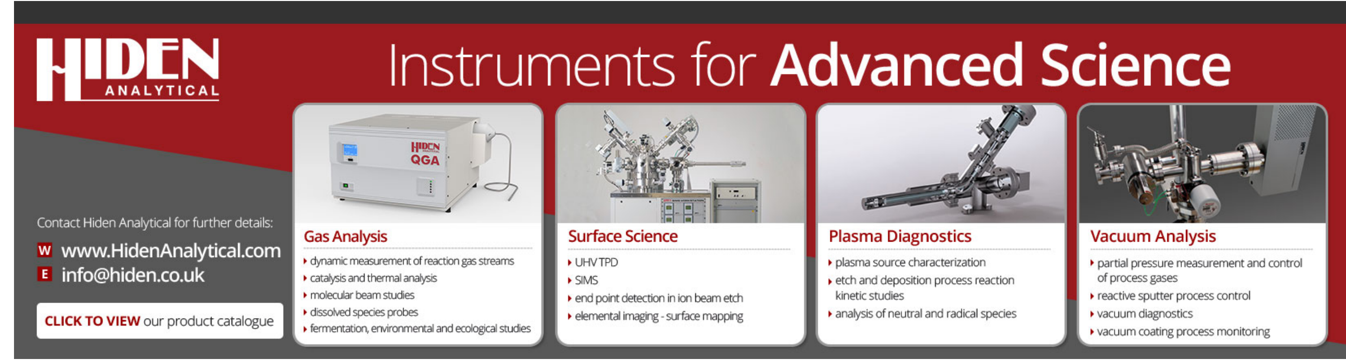

Surface and grain boundary scattering in nanometric Cu thin films: A quantitative analysis including twin boundaries

Katayun Barmak
Department of Applied Physics and Applied Mathematics, Columbia University, New York, New York 10027 and Department of Materials Science and Engineering and Materials Research Science and Engineering Center, Carnegie Mellon University, 5000 Forbes Avenue, Pittsburgh, Pennsylvania 15213

Amith Darbal
Department of Materials Science and Engineering and Materials Research Science and Engineering Center, Carnegie Mellon University, 5000 Forbes Avenue, Pittsburgh, Pennsylvania 15213

Kameswaran J. Ganesh and Paulo J. Ferreira
Materials Science and Engineering, The University of Texas at Austin, 1 University Station, Austin, Texas 78712

Jeffrey M. Rickman
Department of Materials Science and Engineering and Department of Physics, Lehigh University, Bethlehem, Pennsylvania 18015

Tik Sun, Bo Yao, Andrew P. Warren, and Kevin R. Coffey[a)]
Department of Materials Science and Engineering, University of Central Florida, 4000 Central Florida Boulevard, Orlando, Florida 32816

(Received 2 July 2014; accepted 18 August 2014; published 5 September 2014)

The relative contributions of various defects to the measured resistivity in nanocrystalline Cu were investigated, including a quantitative account of twin-boundary scattering. It has been difficult to quantitatively assess the impact twin boundary scattering has on the classical size effect of electrical resistivity, due to limitations in characterizing twin boundaries in nanocrystalline Cu. In this study, crystal orientation maps of nanocrystalline Cu films were obtained via precession-assisted electron diffraction in the transmission electron microscope. These orientation images were used to characterize grain boundaries and to measure the average grain size of a microstructure, with and without considering twin boundaries. The results of these studies indicate that the contribution from grain-boundary scattering is the dominant factor (as compared to surface scattering) leading to enhanced resistivity. The resistivity data can be well-described by the combined Fuchs–Sondheimer surface scattering model and Mayadas–Shatzkes grain-boundary scattering model using Matthiessen's rule with a surface specularity coefficient of $p = 0.48$ and a grain-boundary reflection coefficient of $R = 0.26$. © *2014 American Vacuum Society*.
[http://dx.doi.org/10.1116/1.4894453]

I. INTRODUCTION

The resistivity of polycrystalline metallic thin films increases when film dimensions are of the order of the electron mean-free path, due to surface and grain-boundary scattering of electrons. This phenomenon, first observed by Thomson in 1901, is known as the classical resistivity size effect.[1] Determining the relative contributions of surface and grain-boundary scattering toward this resistivity increase is an important step toward a quantitative understanding of the classical size effect.[2–19]

A commonly used description for the surface scattering contribution to the resistivity increase is the Fuchs–Sondheimer (FS) model.[18] In this model, the resistivity increase is a result of diffuse scattering of conduction electrons at the conductor's exterior surfaces with a probability of $1 - p$, where p ($0 \le p \le 1$) is a specular scattering coefficient that is typically inferred from experimental data. An electron that scatters diffusely loses the additional momentum it has gained from the electric field and leaves the surface in a random direction. An electron that scatters specularly does not change its momentum in the plane parallel to the surface, which includes the direction of the electric field. Thus, specular scattering does not contribute to increased resistivity. The FS expression for the resistivity, ρ_{FS}, of a thin film is[18]

$$\rho_{FS} = \rho_i \left[1 - \left(\frac{3}{2k}\right)(1-p)\int_1^{\infty}\left(\frac{1}{t^3} - \frac{1}{t^5}\right)\frac{1-\exp(-kt)}{1-p\exp(-kt)}dt \right]^{-1}, \quad (1)$$

where $k = h/\lambda$, h is the film thickness, λ is the temperature-dependent electron mean free path, and ρ_i is the bulk resistivity of the metal. Thus, the resistivity increase predicted by this model is $\Delta\rho_{FS} = \rho_{FS} - \rho_i$.

To describe the contribution of grain-boundary scattering to the resistivity, the Mayadas–Shatzkes (MS) model is commonly employed.[19] This model assumes that grain boundaries are all either parallel or perpendicular to the direction of current flow, and that electrons incident upon the parallel

a)Electronic mail: kb2612@columbia.edu

 © 2014 American Vacuum Society

grain boundaries are only specularly reflected, i.e., parallel grain boundaries have no role in the resistivity size effect. Each perpendicular grain boundary is treated as an internal surface, and when a conduction electron collides with the grain boundary, it has a probability of transmission or reflection that is quantified by a reflection coefficient, R. This coefficient takes values between zero and one and is commonly varied to fit experimental data. The resistivity of the film, ρ_{MS}, is given by[19]

$$\rho_{MS} = \rho_i \left[1 - \frac{3}{2}\alpha + 3\alpha^2 - 3\alpha^3 \ln\left(1 + \frac{1}{\alpha}\right)\right]^{-1}, \quad (2)$$

where $\alpha = \left(\frac{\lambda}{g}\right)\frac{R}{(1-R)}$ and g is the average grain size. Using the MS model, the increase in resistivity due to grain-boundary scattering is $\Delta\rho_{MS} = \rho_{MS} - \rho_i$.

Recent studies by Sun *et al.*[11–13] on encapsulated polycrystalline Cu thin films have revealed grain-boundary scattering to be the dominant factor contributing to resistivity increases related to the classical size effect. These studies also show a weaker, but still significant, contribution from surface scattering. Furthermore, it is also observed that a simple summing of the FS model for surface scattering with the MS model for grain-boundary scattering provides the best quantitative description for the classical resistivity size effect in polycrystalline Cu films. For this combined FS + MS model, Sun *et al.*[13] found $p = 0.52$, and $R = 0.43$.

The conclusion reached by Sun *et al.*[13] that grain-boundary scattering is the dominant scattering mechanism when compared with surface scattering was in agreement with earlier studies of the size effect in Cu films with well-controlled grain size and different thickness.[4,5,9] Brongersma *et al.*[4] reported a value of $R = 0.46$, which also compares well with the value of $R = 0.43$ reported by Sun *et al.*[13] It is also worth noting that the film resistivities reported by Sun *et al.*[13] were comparable to the lower resistivities of the electroplated Cu films rather than the higher resistivities of the self-ionized plasma-deposited Cu films reported by Brongersma *et al.*[4] Additionally, in a later study, Barmak *et al.*[15] showed that the values of $p = 0.52$ and $R = 0.43$ obtained by Sun *et al.*[13] could be used to satisfactorily describe the resistivity of Cu wires reported in a representative set of studies from 2002 to 2010, assuming that the impurity content and the grain size/width ratio were varied. This finding was qualified by the facts that, in several of the prior studies, the impurity content was not measured and was viewed as an adjustable variable, and that the grain size, if actually measured rather than assumed equal to the sample line width, was not measured for statistically significant populations of grains. In addition, prior studies did not make clear what measure of grain size was used, a point that will be discussed in more detail in Sec. III. Barmak *et al.*[15] and Sun *et al.*[13] used the same measures of goodness-of-fit in their respective studies, namely, the sum squared error (SSE) and the Bayesian information criterion (BIC) (described in later section), and in several cases, it was found that the fits to the reported data using the values of p and R of Sun *et al.* provided a better fit to the data than the values of p and R given in the original reports, even when the authors concluded that surface scattering was dominant.[14]

One question that was not answered in the Sun *et al.*[11–13] analysis, however, was whether twin boundaries in Cu contribute significantly to the measured resistivity. Due to the difficulty of characterizing twin boundaries in Cu at the nanoscale, this contribution was ignored in these earlier studies. However, given the abundance of twin boundaries in Cu films and the lack of experimental data as to their role in electrical conduction, it is essential to determine their relative importance in electron scattering. Thus, the current work provides a quantitative assessment of the relative importance of dominant scattering mechanisms including the role of twin boundaries. Our report will describe the contributions of various extended defects to electron scattering in Cu, using a statistical analysis of resistivity models that goes well beyond the earlier work of Sun *et al.*[11–13]

Twin boundaries, denoted as $\Sigma3$ boundaries in the coincident site lattice description of grain boundaries,[20] are special interfaces with a specific orientation relationship between the grains. In the angle-axis description, this orientation relationship is a rotation of 60° about the $\langle 111 \rangle$ crystallographic axis. A $\Sigma3$ boundary is classified as a coherent twin boundary if the boundary plane is $\{111\}$; otherwise, the boundary is referred to as an incoherent $\Sigma3$ boundary. (The designations "$\Sigma3$" and "twin" boundaries are used interchangeably in the remainder of the paper.)

With recent developments in automated electron diffraction analysis techniques for the transmission electron microscope (TEM), it is now possible to obtain high-spatial resolution crystal orientation images of nanocrystalline films and to identify the twin boundaries.[21–23] These high-resolution maps are used in the present study to characterize grain boundaries in nanocrystalline Cu films that were previously reported by Sun *et al.*[11–13] Using these results, the resistivity results of Sun *et al.*[13] are reanalyzed to determine the relative contribution of surface and grain-boundary scattering, including contributions from $\Sigma3$ boundaries. It is shown that, in agreement with the work of Sun *et al.*,[11–13] the relative contribution from grain-boundary scattering is predominant, and that the resistivity data is well described by the combined FS surface scattering model and MS grain-boundary scattering model using Matthiessen's rule. However, a slightly lower surface specularity coefficient, $p = 0.48$, and a significantly lower grain boundary reflection coefficient, $R = 0.26$, results when taking all boundaries, including twin boundaries, into account.

II. EXPERIMENTAL METHODS

A. Thin film deposition and characterization

Detailed descriptions of the thin-film deposition technique, and thickness, grain structure, and resistivity characterization methods are available elsewhere.[11–13] Briefly, the Cu films were sputter-deposited on Si (100) substrates with a 150 nm thick layer of thermally grown SiO_2 and cooled to −40 °C by contact with a liquid nitrogen cooled Cu plate. The Cu layer was DC-sputtered from a 99.9999% pure Cu

target, and was encapsulated between an underlayer and an overlayer of SiO_2 or Ta/SiO_2. The SiO_2 layer was 20 nm thick, whereas the Ta layer was 2 nm thick. The films encapsulated in SiO_2 were annealed in Ar + 3% H_2 at ambient pressure at 150 or 600 °C for 30 min, or at 400 °C for 6 s using a halogen lamp (rapid thermal annealing). The films encapsulated in Ta/SiO_2 were annealed in Ar + 3% H_2 at 600 °C. The different annealing treatments were intended to obtain a range of grain sizes for a given film thickness. However, heavy voiding or agglomeration for the thinnest films, and the presence of multiple grains through thickness (rather than the columnar grain structure required for the resistivity analysis) for the thicker films limited the range of usable grain sizes for a given film thickness. Nevertheless, though the grain size and layer thickness could not be fully decoupled, the range of grain sizes achieved for a given film thickness and the measurement of grain size for statistically significant populations of grains (412–1518) for each film allowed quantitative assessment of the separate contributions of surface scattering and grain-boundary scattering to the observed resistivity increase. It is this capability that distinguishes the current work and the prior studies of Sun *et al.*[11–13] from other reports of the resistivity size effect in Cu.

The thickness of the films and the roughness of the Cu/SiO_2 interfaces were measured using x-ray reflectivity experiments at the Stanford Synchrotron Radiation Lightsource.[13] The sheet resistance was measured at room temperature and 4.2 K using a dipping van der Pauw geometry four-point probe.[13]

Plan-view TEM samples were prepared using a back-etching technique, by thinning initially with a HF + HNO_3 solution, and subsequently with a diluted HF solution.[24] Crystal orientation was mapped for two of the SiO_2-encapsulated Cu thin films with thicknesses of 36.9 and 46.4 nm in a JEOL 2010F transmission electron microscope operating at 200 kV. ASTAR™ was employed for automated orientation imaging in the TEM.[25] Details of the orientation mapping are given elsewhere.[23] Briefly, in ASTAR, the electron optical system of the microscope is set up so that a small electron probe (here, approximately 5 nm in diameter) illuminates the specimen. As the nanosized beam is scanned over the specimen, the diffraction pattern is acquired from each point over a square scan area. The scanned area for the current studies was $1440 \times 1440\,nm^2$ in size. Orientation images from 20 and 14 such scan areas were acquired for the 46.4- and 36.9-nm thick Cu films, respectively, to ensure adequate statistical sampling of the microstructure. The electron beam was processed with a semiangle of 0.4° about the optical axis as it was scanned over the specimen to reduce strong dynamical effects in the electron diffraction data that were collected.[26,27] The acquired diffraction patterns were indexed to determine the crystal orientation in an automated manner using a cross-correlation technique to find the best matching solution from a set of precalculated templates. Figure 1 shows a representative color-coded inverse pole figure map in the film normal direction from the Cu films.

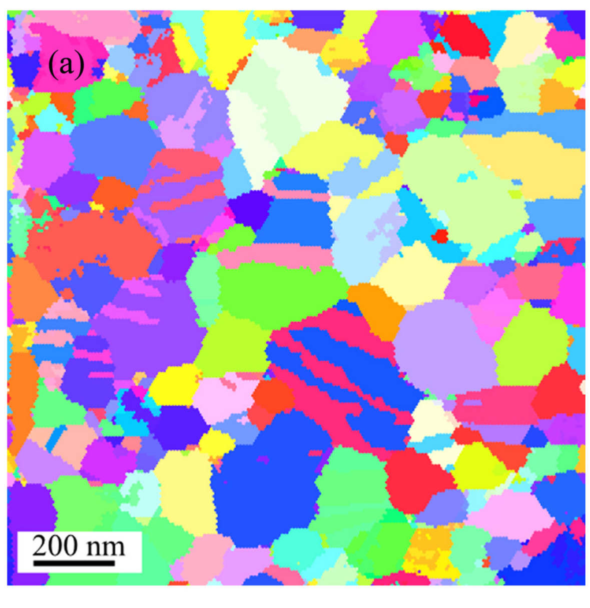

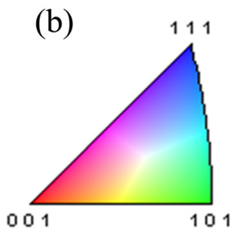

FIG. 1. (Color online) (a) Representative color-coded inverse pole figure map along the film normal direction from the 46.4nm thick Cu film, and (b) color-code for the inverse pole figure map. Reprinted with permission from A. D. Darbal et al., "Grain boundary character distribution of nanocrystalline Cu thin films using stereological analysis of transmission electron microscope orientation maps," Micros. Microanal. **19**, 111–119 (2013). Copyright 2013 Microscopy Society of America.

B. Microstructural analysis

Further analysis of the orientation maps was carried out using the TSL™ OIM data analysis software to identify grains and the types of boundaries separating adjoining grains.[28] In particular, grains were identified using a grouping algorithm in which two neighboring points are considered to be part of the same grain if the disorientation angle (i.e., the minimum misorientation angle) between the two is less than 10°.[28] Boundary segments, generally referred to as reconstructed boundaries, separating adjoining grains were obtained by joining the triple junctions. Since grain boundaries are curved, multiple line segments were used to fit the grain boundary when the distance between the grain boundary and the line segment joining the triple junction was more than 4 pixels. The reconstructed boundary map corresponding to Fig. 1 is displayed in Fig. 2, which shows coherent and incoherent $\Sigma3$ boundaries, as well as non-$\Sigma3$ boundaries. However, in determining the impact of twin boundaries on resistivity, no distinction was made between coherent and incoherent $\Sigma3$ boundaries, and boundary segments were simply categorized as either $\Sigma3$ or non-$\Sigma3$.[29–34] Reconstructed grain-boundary maps from the two samples without twin boundaries were also extracted by excluding all boundaries within a tolerance of 5° of the $\Sigma3$ misorientation. These

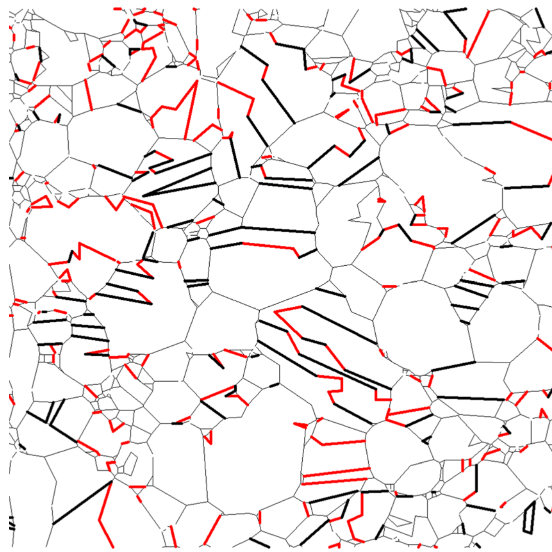

FIG. 2. (Color online) Reconstructed boundary network corresponding to the orientation image shown in Fig. 1 with thick black lines showing coherent twin boundaries and thick red lines showing incoherent twin boundaries.

maps were used to obtain the grain size using Image J.[35] The edge grains were excluded in determining grain size.

For a collection of grains N grains, Sun *et al.*[11–13] used the equivalent circle diameter, $D_{\bar{A}}$, of mean area, $\bar{A} = \sum A_i/N$,

$$D_{\bar{A}} = \sqrt{\frac{4\bar{A}}{\pi}} \quad (3)$$

as the measure of grain size.[11–13] In the current study, the mean intercept length is described as

$$\bar{L} = \pi \frac{\sum A_i}{\sum C_i}, \quad (4)$$

where A_i (C_i) is the area (perimeter) of each of the grains in the aggregate.[36,37] $\bar{L}$ was used because grain shapes are no longer equiaxed when twin boundaries are present and because twin boundaries do not always meet at triple junctions.[36,38] (Note that the total circumference of grains is twice the boundary length since each boundary is measured separately for each of the two adjoining grains when using Image J.) Equation (2) was used to determine the mean intercept length for the Cu films reported by Sun *et al.*[13] This allowed a simple relationship to be derived between the two grain-size parameters, namely, $\bar{L}^{\mathrm{HCDF}} = r_1 D_{\bar{A}}^{\mathrm{HCDF}}$, where $r_1 = 0.76 \pm 0.02$ and HCDF denotes the hollow-cone dark-field method of imaging in the scanning transmission electron microscope.

To assess the different methodologies for determining mean grain size, the equivalent circle diameters $D_{\bar{A}}^{\Sigma 3x}$ (where $\Sigma 3x$ denotes the exclusion of twin boundaries) obtained from the orientation maps are given in Table I for the two films studied along with $D_{\bar{A}}^{\mathrm{HCDF}}$, the latter as reported by Sun *et al.*[13] It was found that, within the allowed variation on the mean grain size based on the population, the grain size values from the orientation maps, $D_{\bar{A}}^{\Sigma 3x}$, were equal to the mean grain sizes, $D_{\bar{A}}^{\mathrm{HCDF}}$, from Sun *et al.*[13] for the two films, i.e., $D_{\bar{A}}^{\Sigma 3x} = D_{\bar{A}}^{\mathrm{HCDF}}$, and therefore the two methods for obtaining the mean grain size can be considered as equivalent. This result then also implies that $\bar{L}^{\Sigma 3x} = \bar{L}^{\mathrm{HCDF}}$.

It remains to obtain a measure of the average grain size (i.e., mean intercept length) that includes twin boundaries, $\bar{L}^{all}$ (Fig. 3). Given that $\bar{L}^{\Sigma 3x} = \bar{L}^{HCDF}$, an estimate of $r_2 = \bar{L}^{all}/\bar{L}^{\Sigma 3x}$ is therefore required. The relevant quantities, obtained from the reconstructed grain-boundary maps, are given in Table I for the mapped Cu films. Also given in Table I is the relevant ratio, r_2, for the two samples measured. For the purposes of this work we calculate $r_2 = 0.63$, which is an average of the values for the two microstructures. The result is

$$\bar{L}^{\mathrm{all}} = r_2 \bar{L}^{\Sigma 3x} = r_2 \bar{L}^{HCDF} = r_2 r_1 D_{\bar{A}}^{HCDF} = 0.48 D_{\bar{A}}^{HCDF}. \quad (5)$$

Finally, Eq. (3) was used to obtain the average grain size as mean intercept length that includes twin boundaries, $\bar{L}^{all}$, from the equivalent circle diameters of mean area $D_{\bar{A}}^{\mathrm{HCDF}}$ for the 22 Cu films reported by Sun *et al.*[13] $\bar{L}^{all}$ is plotted as a function of film thickness in Fig. 3.

C. Statistical analysis

Sun *et al.*[13] evaluated nine resistivity models to account for various combinations of roughness, and surface and grain-boundary scattering in analyzing the resistivity data of their 22 Cu films measured both at room temperature and at liquid helium temperature. Their models had between zero and three adjustable parameters. As increasing the number of adjustable parameters leads to lower errors and to improved goodness-of-fit, Sun *et al.*[13] used the BIC[39] in addition to SSE to compare the models and to select the model that best described the room-temperature and liquid helium temperature resistivities of their Cu films. The BIC incorporates a penalty term for an increased number of adjustable parameters, and is therefore a suitable criterion for comparing models with different numbers of adjustable parameters. The BIC they employed, with the assumption of normally distributed errors, was[39]

$$\begin{aligned} \mathrm{BIC} &= -2 \times \ln(L) + a \ln(n) \\ &= n \ln\left(\frac{SSE}{n}\right) + n \ln(2\pi) + n + a \ln(n), \end{aligned} \quad (6)$$

TABLE I. Cu layer thickness, the number of grains measured, and the equivalent circle diameter of mean area, $D_{\bar{A}}^{\mathrm{HCDF}}$, reported by Sun *et al.* (Ref. 13) are given, in addition to the number of grains measured, the equivalent circle diameters of mean area and mean intercept lengths excluding and including twin boundaries, ($D_{\bar{A}}^{\Sigma 3x}$, $D_{\bar{A}}^{\mathrm{all}}$, $\bar{L}^{\Sigma 3x}$, and $\bar{L}^{\mathrm{all}}$, respectively) calculated from the crystal orientation maps. The ratio of $\bar{L}^{\mathrm{all}}/\bar{L}^{\Sigma 3x}$ is also given. See text for more details.

Thickness (nm)	Grains measured	$D_{\bar{A}}^{\mathrm{HCDF}}$ (nm)	Grains measured	$D_{\bar{A}}^{\Sigma 3x}$ (nm)	$\bar{L}^{\Sigma 3x}$ (nm)	Grains measured	$D_{\bar{A}}^{\mathrm{all}}$ (nm)	$\bar{L}^{\mathrm{all}}$ (nm)	$r_2 = \frac{\bar{L}^{\mathrm{all}}}{\bar{L}^{\Sigma 3x}}$
36.9	576	81 ± 5	3841	78 ± 3	65 ± 2	7197	57 ± 1	43 ± 1	0.66 ± 0.03
46.4	419	113 ± 8	1941	112 ± 6	93 ± 5	5577	77 ± 2	57 ± 1	0.61 ± 0.03

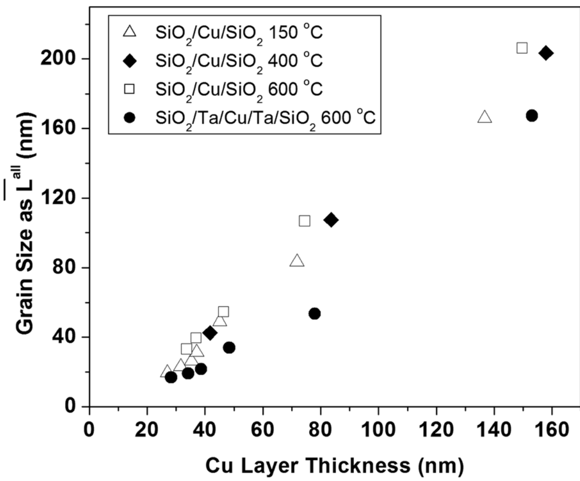

FIG. 3. Average grain size as mean intercept length including twin boundaries, $\bar{L}^{\text{all}}$, obtained using Eq. (3) and the equivalent circle diameters of mean area, $D^{\text{HCDF}}_{\bar{A}}$, reported in Sun *et al.* (Ref. 13), are plotted as a function of Cu layer thickness.

where L is the overall likelihood (i.e., the product of the likelihoods for each of the measurements), a is the number of adjustable or fitting parameters, n is the number of experimental measurements ($n = 44$, 22 measurements at each of two temperatures for the work of Sun *et al.*[13]), and

$$\frac{\text{SSE}}{n} = \sigma^2 = \frac{\sum_{i=1}^{n}\left(\rho_i^{\text{experiment}} - \rho_i^{\text{model}}\right)^2}{n}.$$

For this formulation of the BIC, "good" models have negative BIC's and, the lower the BIC, the better the model. The magnitude of the difference between the BIC values of two models must be greater than two for one model to be considered a better predictor of the experimental behavior than another; otherwise, the distinction between the two models is not significant.

In the current work, in order to determine the optimal values of the adjustable parameter p, a forward modeling approach was employed to arrive at the global minimum of SSE that provided a more accurate result for the shallow minima in SSE than the fitting approach used by Sun *et al.*[13] As a result, the optimal values of the parameters differed in some cases from the values given by Sun *et al.*[13] These differences were, however, small, and do not affect the conclusions reached in Sun *et al.*[13]

For the forward modeling approach, the values of p and R were varied in steps of 0.01 from 0.01 to 0.99 and the errors, $E = \rho_i^{\text{experiment}} - \rho_i^{\text{model}}$, were calculated for each of the 44 experimental resistivity results over the full grid of p and R. The error values for the minimum SSE were used to determine the BIC using Eq. (4). As was the case in Sun *et al.*,[13] the experimentally measured[40] resistivity of bulk Cu, ρ_i, as a function of temperature was used throughout to calculate the temperature-dependent mean-free path (arising from phonon scattering) for the conduction electrons using the relationship: $\rho_i\lambda = 6.6\times10^{-16}\ \Omega\text{m}^2$.

The independent and coupled errors in p and R in the FS + MS model were determined via the bootstrap resampling method of statistical analysis using 10 000 resamplings on the 44 squared error values to obtain the SSE at the 95% confidence level.[41] Briefly, in one resampling step employing this method, a new set of 44 squared error values is selected randomly, one at a time, from the original set and a new SSE is calculated using this new set. The resampling was repeated 10 000 times and the distribution of SSEs was plotted and the SSE at the 95th percentile was employed to determine the errors on p and R.

III. RESULTS AND DISCUSSION

The model parameters, the SSE, and the BIC values for the FS + MS model are given in Table II for two cases: the first in which twin boundaries are excluded and the measure of grain size is the equivalent circle diameter of mean area ($D^{\text{HCDF}}_{\bar{A}}$); and the other in which twin boundaries are included and the measure of grain size is the mean intercept length ($\bar{L}^{\text{all}}$). Table II shows that a SSE value of 0.48 is obtained for the FS + MS model, whether twin boundaries are excluded[8] or not. The BIC values obtained for these cases are −66.2 and −66.5, respectively. These values are also essentially identical, irrespective of twin boundary inclusion. Using the forward modeling approach, the optimal values of p and R are, respectively, 0.55 and 0.43, excluding twin boundaries, and 0.48 and 0.26, including twin boundaries.

The independent and coupled ranges of error at 95% confidence on the SSE using the bootstrap method are given for p and R in Table III and plotted in Fig. 4. As can be seen from the table and the figure, the error range for p is significantly larger than that for R. For the independent errors, the error range for p is ±0.13, whereas for R it is ±0.01 (±0.02) when excluding (including) twin boundaries. When the coupled error is considered, the error ranges for both p and R increase up to as great as 0.32 for p and 0.04 for R. These error ranges and an examination of Fig. 4 indicate a shallow minimum along p, but a sharp minimum along R.

TABLE II. Model, the number of adjustable parameters, optimized model parameters of p, surface specularity, and R, grain boundary reflection coefficient, SSE, and the BIC calculated using Eq. (4). Model parameters and the associated SSE and BIC are given for two measures of grain size. $D^{\text{HCDF}}_{\bar{A}}$ is grain size as equivalent circle diameter of mean area excluding twin boundaries reported by Sun *et al.* (Ref. 13). $\bar{L}^{\text{all}}$ is grain size as mean intercept length including twin boundaries, obtained using crystal orientation mapping. See text for more details.

		Grain size as $D^{\text{HCDF}}_{\bar{A}}$ (Ref. 13)			Grain size as $\bar{L}^{\text{all}}$ (this work)		
Model	Number of parameters, a	Model parameter(s)	SSE ($\mu\Omega^2$ cm^2)	BIC	Model parameter(s)	SSE ($\mu\Omega^2$ cm^2)	BIC
FS + MS	2	$p = 0.55$ $R = 0.43$	0.48	−66.2	$p = 0.48$ $R = 0.26$	0.48	−66.5

TABLE III. Model parameters, p and R, and independent and coupled errors in these parameters for the FS + MS model. The errors are determined via the bootstrap resampling method. See text for more detail.

Grain size as $D_{\bar{A}}^{HCDF}$		Grain size as $\bar{L}^{all}$	
Independent	Coupled	Independent	Coupled
$p = 0.55 \pm 0.13$, $R = 0.43 \pm 0.01$	$p = 0.55(+0.24/-0.30)$, $R = 0.43(+0.02/-0.04)$	$p = 0.48 \pm 0.13$, $R = 0.26 \pm 0.02$	$p = 0.48(+0.32/-0.23)$, $R = 0.26(+0.03/-0.02)$

We can now compare quantitatively the surface scattering coefficients for the two cases, excluding and including twin boundaries, using an average coupled error bar for p of 0.27 (see Table III). Given the scattering coefficients 0.55 ± 0.27 and 0.48 ± 0.27 for the cases excluding and including twin boundaries, respectively, a t-test allows us to conclude that these two values are essentially the same at a level of significance of 0.05. This, in turn, implies that the surface scattering contribution to the resistivity increase is approximately the same for both cases. With regard to the grain-boundary scattering, using $R = 0.26$, the contribution to the overall resistivity of the films is found to be 88%, on average. Therefore, we can conclude that, in agreement with Sun *et al.*,[13] grain-boundary scattering is the dominant scattering mechanism affecting the resistivity of nanocrystalline Cu films with grain sizes and thicknesses that are approximately equal to or greater than the electron mean free path of Cu at room temperature.

The values $R = 0.26$, including twin boundaries, and $R = 0.43$, excluding twin boundaries, compare well with the range of calculated values obtained by Feldman *et al.*[34] based on a Green's function formalism for twin and nonboundaries in Cu. The values of $p = 0.48$ and $R = 0.26$ obtained in the current study also compare well with the values reported in Josell *et al.*[10] of $p = 0.55$ and $R = 0.20$ based on a chi-squared fit of model predictions to the resistivity data of Cu lines. However, despite these favorable comparisons, there is one issue that is worth addressing, as noted in the Introduction. In most, if not all studies, except this work and that of Sun *et al.*,[13] the grain size is either not measured and assumed equal to a sample structural dimension (e.g., film thickness or line width) or is not measured for statistically significant populations. Moreover, in cases where grain size is measured, it is unclear which measure of grain size is used. Beyond the measures indicated above, namely, $D_{\bar{A}}$ and $\bar{L}$, a third measure is the mean equivalent circle diameter, $\bar{D}$, wherein the equivalent circle diameter is found for each grain, from which the mean diameter for the population of grains is obtained. Using these different measures, different values for R will be found.

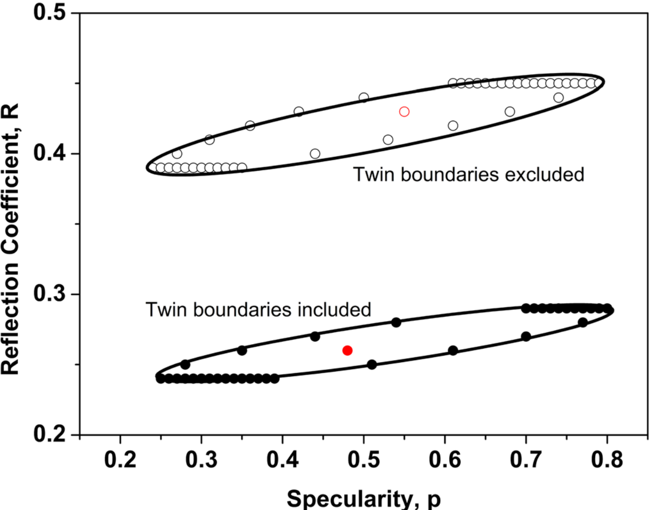

FIG. 4. (Color online) Reflection coefficient, R, is plotted vs the surface specularity, p, to show the error range on p and R at 95% confidence on the SSE obtained using the bootstrap method of resampling. The values of p and R that give the minimum SSE are marked with open and closed red circles, respectively. The ovals are drawn to guide the eye.

To give a concrete example, Chen *et al.*[30] reported the resistivity of a series of ultrafine-grained and twinned Cu samples obtained by pulse electroplating. They found lower resistivity with increasing twin boundary content, and argued that the nature of grain boundaries (excluding twin boundaries) changed as the twin content increased. They reported values of R *excluding* twin boundaries of 0.23, 0.53, and 0.66 for three different samples having twin widths of 15, 35, and 90 nm, respectively. However, they did not note which measure of grain size was used. Sun *et al.*[13] reported a value of $R = 0.43$, excluding twin boundaries, using an equivalent circle diameter of mean area. By contrast, if $\bar{L}$ is used, the result is $R = 0.36$, whereas using $\bar{D}$ results in $R = 0.41$ (excluding grain boundaries). It is noted that, irrespective of measure of grain size, the values obtained for R for the films of Sun *et al.*[13] are well within the range of 0.23–0.66 reported by Chen *et al.*[30] This discussion, however, underlines the need for explicit mention of the "measure of grain size" and the need to measure grain size for statistically significant populations in future studies of the resistivity size effect.

The last point warranting discussion is that Sun *et al.*,[13] and therefore by extension the work reported here, found no difference in the surface specularity, p, between the Cu/SiO_2 and Cu/Ta interfaces. Other reports indicate that there should be a difference, an excellent example of which is the work of Rossnagel and Kuan.[6] In their work, deposition of Ta on pseudoepitaxial Cu deposited on (110) Si resulted in an increase in resistivity. However, once Ta was allowed to oxidize in air, the film resistivity reduced back to the value for an uncoated film. It is therefore entirely plausible that in the work of Sun *et al.*[13] the encapsulating Ta layers oxidized during film annealing, despite the use of a reducing $Ar\text{-}H_2$ ambient, resulting in indistinguishably different specularity parameters for Cu/SiO_2 and Cu/Ta interfaces.

IV. SUMMARY AND CONCLUSIONS

Crystal orientation maps in the transmission electron microscope were used to characterize grain boundaries in

nanocrystalline Cu films. Using the crystal orientation maps, grain size was obtained as the mean intercept length, including twin boundaries. These grain size values were used to determine the relative contributions of surface scattering and grain-boundary scattering to the resistivity size effect observed in the films. It was shown that the contribution from grain-boundary scattering is the dominant factor (as compared to surface scattering) toward the resistivity increase. The resistivity data were well-described by the combined Fuchs–Sondheimer surface scattering model and Mayadas–Shatzkes grain-boundary scattering model using the Matthiessen's rule (FS + MS) with a surface specularity coefficient $p = 0.48(+0.32/-0.23)$ and a grain-boundary reflection coefficient $R = 0.26(+0.03/-0.02)$ obtained by minimization of sum squared errors. The error ranges for p and R were obtained using the bootstrap resampling method. It was observed that the error range for p is significantly larger than that for R.

ACKNOWLEDGMENTS

Financial support of the SRC, Task 1292.008 and 2121.001, and of the MRSEC program of the NSF under DMR-0520425 is gratefully acknowledged. E. Rauch is thanked for helpful discussions, and X. Liu is thanked for assistance with Fig. 4.

[1]J. J. Thomson, Proc. Cambridge Philos. Soc. **11**, 120 (1901).
[2]F. Chen and D. Gardner, IEEE Electron Device Lett. **19**, 508 (1998).
[3]W. Steinhögl, G. Schinlder, G. Steinlesberger, and M. Engelhardt, Phys. Rev. B **66**, 075414 (2002).
[4]S. H. Brongersma *et al.*, IEEE Int. Interconnect Technol. Conf. **2004**, 48.
[5]W. Zhang, S. H. Brongersma, T. Clarysse, V. Terzieva, E. Rosseel, W. Vandervorst, and K. Maex, J. Vac. Sci. Technol., B **22**, 1830 (2004).
[6]S. M. Rossnagel and T. S. Kuan, J. Vac. Sci. Technol,. B **22**, 240 (2004).
[7]W. Steinhögl, G. Schinlder, G. Steinlesberger, M. Traving, and M. Engelhardt, J. Appl. Phys. **97**, 023706 (2005).
[8]J. J. Plombon, E. Andideh, V. M. Dubin, and J. Maiz, Appl. Phys. Lett. **89**, 113124 (2006).
[9]W. Zhang, S. H. Brongersma, Z. Li, D. Li, O. Richard, and K. Maex, J. Appl. Phys. **101**, 063703 (2007).
[10]D. Josell, S. H. Brongersma, and Z. Tőkei, Annu. Rev. Mater. Res. **39**, 231 (2009).
[11]T. Sun, B. Yao, A. Warren, V. Kumar, S. Roberts, K. Barmak, and K. R. Coffey, J. Vac. Sci. Technol., A **26**, 605 (2008).
[12]T. Sun, B. Yao, A. Warren, K. Barmak, M. F. Toney, R. E. Peale, and K. R. Coffey, Phys. Rev. B **79**, 041402(R) (2009).
[13]T. Sun, B. Yao, A. P. Warren, K. Barmak, M. F. Toney, R. E. Peale, and K. R. Coffey, Phys. Rev. B **81**, 155454 (2010).
[14]R. L. Graham, G. B. Alers, T. Mountsier, N. Shamma, S. Dhuey, S. Cabrini, R. H. Geiss, D. T. Read, and S. Peddeti, Appl. Phys. Lett. **96**, 042116 (2010).
[15]K. Barmak, T. Sun, and K. R. Coffey, *Proceedings of the 11th International Workshop on Stress Induced Phenomena, 2010*, edited by E. Zschech, P. S. Ho, and S. Ogawa (AIP Conf. Proc., Melville, New York, 2010), Vol. 1300, pp. 12–22.
[16]J. M. Rickman and K. Barmak, J. Appl. Phys. **112**, 013704 (2012).
[17]J. M. Rickman and K. Barmak, J. Appl. Phys. **114**, 133703 (2013).
[18]K. Fuchs, Math. Proc. Cambridge Philos. Soc. **34**, 100 (1938); E. H. Sondheimer, Adv. Phys. **1**, 1 (1952).
[19]A. F. Mayadas and M. Shatzkes, Phys. Rev. B **1**, 1382 (1970).
[20]S. Ranganathan, Acta Crystallogr. **21**, 197 (1966).
[21]K. J. Ganesh, M. Kawasaki, J. P. Zhou, and P. J. Ferreira, Microsc. Microanal. **16**, 614 (2010).
[22]K. J. Ganesh, A. D. Darbal, S. Rajasekhara, G. S. Rohrer, K. Barmak, and P. J. Ferreira, Nanotechnology **23**, 135702 (2012).
[23]A. D. Darbal *et al.*, Microsc. Microanal. **19**, 111 (2013).
[24]B. Yao and K. R. Coffey, J. Electron Microsc. **57**, 47 (2008).
[25]E. F. Rauch, J. Portillo, S. Nicolopoulos, D. Bultreys, S. Rouvimov, and P. Moeck, Z. Kristallogr. **225**, 103 (2010).
[26]R. Vincent and P. A. Midgley, Ultramicroscopy **53**, 271 (1994).
[27]P. Oleynikov, S. Hovmöller, and X. D. Zou, Ultramicroscopy **107**, 523 (2007).
[28]F. J. Humphreys, J. Mater. Sci. **36**, 3833 (2001).
[29]L. Lu, Y. Shen, X. Chen, L. Qian, and K. Lu, Science **304**, 422 (2004).
[30]X. H. Chen, L. Lu, and K. Lu, J. Appl. Phys. **102**, 083708 (2007).
[31]K. Lu, L. Lu, and S. Suresh, Science **324**, 349 (2009).
[32]C. Goux, Can. Metall. Q. **13**, 9 (1974).
[33]A. Sutton and R. Balluffi, *Interfaces in Crystalline Materials* (Clarendon, Oxford, 1996), p. 27.
[34]B. Feldman, S. Park, M. Haverty, S. Shankar, and S. T. Dunham, Phys. Status Solidi **247**, 1791 (2010).
[35]See http://rsb.info.nih.gov/ij/ for the image analysis software provided by the National Institutes of Health.
[36]E. E. Underwood, *Quantitative Stereology* (Reading, Massachuttes, 1970), p. 4.
[37]S. I. Tomkeieff, Nature **155**, 24 (1945).
[38]J. E. Hilliard and L. R. Lawson, *Stereology and Stochastic Geometry* (Kluwer Academic Publisher, Dordecht, 2003), pp. 125–172.
[39]G. Schwarz, Ann. Stat. **6**, 461 (1978).
[40]D. R. Lide, *CRC Handbook of Chemistry and Physics*, 87th ed. (CRC, Boca Raton, 2006), pp. 12–39.
[41]B. Efron, Ann. Stat. **7**, 1 (1979).